LA-UR-01-4892
Approved for public release; distribution is unlimited.

Title: **Performance of a Novel SQUID-Based Superconducting Imaging-Surface Magnetoencephalography System**

Author(s): R.H. Kraus, Jr., P. Volegov, K. Maharajh, M.A. Espy, A. N. Matlashov, and E.R. Flynn

Submitted to:

http://lib-www.lanl.gov/cgi-bin/getfile?00796810.pdf

Version Date: 9/26/2001 5:03 PM

Performance of a Novel SQUID-Based Superconducting Imaging-Surface Magnetoencephalography System

R.H. Kraus, Jr.[a], P. Volegov[b], K. Maharajh[b], M.A. Espy[a], A. N. Matlashov[a], and E.R. Flynn[c]

[a]Biophysics Group, Los Alamos National Laboratory, Los Alamos NM 87545
[b]Physics and Astronomy Department, University of New Mexico, Albuquerque NM 87201
[c]Senior Scientific, Albuquerque NM 87201

Abstract— Performance for a recently completed whole-head magnetoencephalography system using a superconducting imaging-surface (SIS) surrounding an array of 150 SQUID magnetometers is reported. The helmet-like SIS is hemispherical in shape with a brim. Conceptually, the SIS images nearby sources onto the SQUIDs while shielding sensors from distant "noise" sources. A finite element method (FEM) description using the as-built geometry was developed to describe the SIS effect on source fields by imposing $B_{\perp}$(surface)=0. Sensors consist of 8mm × 8mm SQUID magnetometers with 0.84nT/Φ sensitivity and <3fT/√Hz noise. A series of phantom experiments to verify system efficacy have been completed. Simple dry-wire phantoms were used to eliminate model dependence from our results. Phantom coils were distributed throughout the volume encompassed by the array with a variety of orientations. Each phantom coil was precisely machined and located to better than 25μm and 10mRad accuracy. Excellent agreement between model-calculated and measured magnetic field distributions of all phantom coil positions and orientations was found. Good agreement was found between modeled and measured shielding of the SQUIDs from sources external to the array showing significant frequency-independent shielding. Phantom localization precision was better than 0.5mm at all locations with a mean of better than 0.3mm.

Keywords—Magnetoencephalography, MEG, Source localization, SQUID array.

Corresponding Author—
Dr. Robert H. Kraus, Jr.
Biophysics Group
Los Alamos National Laboratory
MS D454 Los Alamos, NM 87545 USA
Phone: (505) 665-1938
FAX: (505) 665-4507
E-mail: rkraus@lanl.gov

Main Text—

1. Introduction

Weak magnetic fields are a direct consequence of neuronal activity in the brain that causes ionic currents to flow in the neurons[1]. Magnetoencephalography (MEG) is the technique that measures the weak magnetic fields that emanate from the brain[2] as a direct consequence of the neuronal currents resulting from brain activity. The extraordinarily weak magnetic fields, typically 10-100 femtoTesla (fT), are measured by an array of SQUID (Superconducting QUantum Interference Device) sensors. The position and vector characteristics of these neuronal sources can be estimated from the inverse solution of the field distribution at the surface of the head. In addition to locating the sources of neuronal activity, MEG temporal resolution is unsurpassed by any other method currently used for brain imaging. Although MEG is not truly tomographic and source reconstruction is limited by solutions of the electromagnetic inverse problem, constraints used for source localization produce reliable and accurate results. Current MEG instrumental source location accuracy reported in the literature is approximately 2 to 4 mm, depending on source parameters, and typically 5-10 mm accuracy is attained in most medical applications with the latest instruments.

A unique whole-head MEG system incorporating a superconducting imaging-surface (SIS) has been designed and built at Los Alamos with the goal of dramatically improving source localization accuracy while mitigating limitations of current systems (e.g. low signal-to-noise, cost, bulk). The Los Alamos SIS-MEG system[3] is based on the principal that Meissner currents flow in the surface of superconductors, preventing any significant penetration of magnetic fields. A hemispherical SIS with a brim, or helmet, surrounds the SQUID sensors largely shielding them from sources outside the helmet while measuring fields from nearby sources within the helmet.

Localizing sources of neuronal activation from MEG measurements requires a complete description of the "forward physics" describing how neuronal currents lead to magnetic fields at the SQUID sensors. The MEG forward model typically includes the complex neuronal source model that incorporates intracellular ionic currents, intercellular and extracellular volume currents, brain structure, and conductivities. The forward model for the SIS-MEG system must additionally include the effect of the superconducting surface on the fields generated by all of the primary sources as well as fields generated by the Meissner currents in the SIS.

2. Method

An analytic description of the fields at the sensors requires that the homogenous solution corresponding to the free space fields are added to any source(s) and include the superconductor boundary condition. Analytic solutions are known for simple geometries such as the sphere or infinite plane[4], but for finite geometries the field is difficult or impossible to determine analytically. Consequently, we have implemented a finite element model (FEM) description of the SIS forward physics using the exact as-built geometry. The FEM is used to compute the distribution of Meissner currents[5] in the complicated surface geometry that result in a net surface magnetization such that the normal components of the surface magnetization and free space magnetic field are equal and opposite (e.g. $\boldsymbol{B}_{\perp}$(surface)=0). The SIS is divided into a mesh of triangular elements (Fig. 1), each of which is assigned a uniform magnetization. The net magnetic field at each surface element is a superposition of the primary field and the fields produced by all triangular elements. Using the Biot-Savart law to describe the field from each segment of the triangle, summing over all *m* segments, and using collocation method we can write *m* linear equations for I_j:

$$\sum_{j=1}^{m} A_{ij} I_j = -b_i, \quad i = \overline{1,m} \quad \text{and} \quad A_{ij} = \frac{\mu_0}{4\pi} \cdot \mathbf{n}_i \cdot \left(\sum_{k=0}^{2} [\mathbf{r}_{ij}^{(k)} \times \mathbf{r}_{ij}^{(k+1)}] \frac{(r_{ij}^{(k)} + r_{ij}^{(k+1)})}{r_{ij}^{(k)} r_{ij}^{(k+1)} (r_{ij}^{(k)} r_{ij}^{(k+1)} + (\mathbf{r}_{ij}^{(k)} \cdot \mathbf{r}_{ij}^{(k+1)}))} \right)$$

$$b_i = \mathbf{n}_i \cdot \mathbf{B}_p(\mathbf{p}_i), \quad \mathbf{r}_{ij}^{(k)} = \mathbf{p}_i - \mathbf{v}_j^{(k \bmod 3)}$$

where $\mathbf{r}_{ij}$ are the positions from the endpoints to the observer, I_j is equivalent magnetization current for each cell, $\mathbf{B}_p$ is primary (free space) magnetic field resulting from a current density **J**, $\{\mathbf{p}_i\}_1^m$ are points at the center of each ith cell, and $\mathbf{n}_i$ is the unit vector normal to the surface at the ith cell.

The SIS is fabricated from lead (Type I superconductor at 4K) consisting of a 5.064-inch radius hemisphere with two small "cut-outs" at opposite sides of the hemisphere, and a 2-inch brim that is smoothly melded to the edge of the modified hemisphere. An array of 150 SQUID magnetometers is mounted on "studs" at offsets from the SIS ranging from 1cm to 3cm and operated in a liquid helium bath at ~4K. The SQUID-SIS offsets were allowed to vary in order to minimize sensor to warm dewar surface (and consequently the subject head) distance. The 2734 element FEM mesh, shown in Fig. 1, includes all aspects of the SIS such as the hemispherical core, cut-outs for the ears, and brim with approximately equal sized elements over the entire geometry.

A precision multi-source phantom was constructed to generate well-characterized source fields to test the FEM approach and MEG system. Simple dry-wire phantoms, for which the source model can be completely described, were used to eliminate any source model dependence from our results. The 25-coil phantom distributed sources throughout the volume encompassed by the array. Three orthogonal coils were located at most positions to study effects of source orientation. Each phantom coil was precisely machined and located relative to the phantom 'origin' with an absolute precision better than 25μm and 10mRad. The *a priori* phantom position relative to the SQUID array is known to ~±1cm. Cooling the sensor array from ~300K to 4K causes significant symmetric and asymmetric contractions; consequently we assumed initial ±1mm and ±100mRad sensor position and orientation accuracy. SQUID sensitivities were calibrated to 0.5% accuracy prior to installation, however a systematic error discovered later may increase the error to 1%.

Phantom source coils were activated using a sinusoidally driven constant-current supply (<0.5% absolute error and <0.1% stability) at 77.15Hz. Data were acquired by simultaneous sampling 24-bit delta-sigma digitizers at 3 kSa/sec with high-pass filters disabled and low-pass anti-aliasing filters at 1.2kHz. The raw data were digitally filtered using a narrow (<0.01Hz) band-stop algorithm that produced minimal artifacts and implemented in MATLAB. A 2.5m diameter double-Helmholtz coil set[6] was also constructed to generate a uniform field distribution. The uniform field coil set and a dipole coil located ~2m from the SIS helmet were activated at a variety of frequencies to test the shielding performance of the SIS.

3. Results

Shielding of the SQUIDs from sources external to the array was both modeled and measured for point dipole (2m from the SIS helmet center) and uniform field sources. We observed shielding factors for sensors above the SIS brim varying from 50 to 200. Sensors nearest the SIS edge experienced the poorest shielding varying between 15 and 30. Shielding factors were experimentally verified to be independent of frequency from DC to 1kHz, limited by our sampling frequency. Trends in experimentally measured shielding factors agreed well with model predictions, however discrepancies in shielding factors of up to 50% were observed and attributed to the pervasive presence of magnetic materials in our laboratory that could not be readily modeled. A vector representation of fields computed at each SQUID for external sources are shown in Fig. 2. It is immediately apparent that sensors closest to the SIS edge, especially near the ear cut-outs, are most sensitive to sources outside the SIS and the shielding factor for these sensors is quite sensitive to the specific source field distribution.

Signals were measured from each phantom coil by all SQUID sensors in the array. An inversion of the data from one set of 25 phantom locations was performed to localize each sensor in space and orientation. This is conceptually opposite to but mathematically identical to inversion of sensor array data to localize a source. The unique procedure was used to calibrate the position of each sensor at 4K, compensating for machining errors, effects of thermal contraction, and sensor calibration errors. After calibrating the sensor array, an independent set of phantom data were acquired at typical S/N=20 (100-500fT signal amplitude). Source localization of phantom coils was performed using our source/SIS forward physics and the calibrated SQUID positions and sensitivities.

A representative sample of the calculated and measured fields for the phantom coils is shown in Figure 3 where the fields for two sets of three orthogonal coils are illustrated for locations near the apex of the SIS and near the periphery. Each coil set consisted of one approximately radial to the SIS and two roughly tangential to the SIS and orthogonal to one another. Inspection of Figure 3 shows extremely good agreement between model and experimental field distributions. Differences between measured and computed fields were less than 1% for all sensors for which any significant field was measured. A recently discovered coil-to-coil variation in phantom field strength (by as much as 3%) may explain at least part of the discrepancy since all coils were assumed to be identical.

The impact of spatially calibrating the SQUID sensor array is evident in the phantom source localization results. Prior to calibrating sensor locations, the mean source localization error was ~1mm with the maximum error ~4mm (Figure 4). After calibrating the sensor locations, the means source localization error was <0.2mm with the maximum error of 0.45mm (Figure 5). Inverse source localization was performed to locate each of the 50 phantom coils and resulted in a mean error of less than 0.3 millimeters. The accuracy of source localization for our system was independent of source orientation.

4. Conclusions

All results computed using our FEM approach agree extremely well with measured field distributions at the SQUID sensor array for sources inside and outside the SIS helmet. Discrepancies between the measured and computed results, though small, are primarily attributed to finite mesh size and the fact that a precise calibration of phantom source strength had not been performed. We have found that a FEM approach provides a powerful and robust method for describing the effect of an arbitrarily shaped SIS on magnetic field distributions. The FEM description of the SIS helmet will become an integral part of the forward physics description of the Los Alamos

MEG system. Fields from external sources (noise) were typically reduced by approximately two orders of magnitude across all frequencies. This reduction was less for sensors near the edge of the SIS helmet, as expected, and depended on the details of the noise source. We also report that the SIS-MEG system has an effective "instrumental" source localization accuracy of better than 0.5mm, and typically 0.3mm for well characterized sources. This source localization accuracy was observed throughout the volume inside the SIS helmet, including regions near the periphery of the sensor array.

The ultimate goal of the SIS-MEG system is to precisely localize sources within a human brain. A detailed understanding of how various measurement and modeling errors impact source localization must be obtained in order to accurately compare SIS results with those reported in the literature. More importantly, this understanding is crucial to relating how localization results for simple phantoms (such as the one used here) compare with complex 'real-world' sources such as the human brain.

Acknowledgements—The Authors gratefully acknowledge support from the US National Institutes of Health (NINDS), Department of Energy (OBER), and the National Foundation for Functional Brain Imaging.

References—

[1] Okada, Y., "Neurogenesis of evoked magnetic fields", Biomagnetism, an interdisciplinary approach, Eds.: Williamson, S. J., et al, Plenum (1983)
[2] Hämäläinen, M., Hari, R., Ilmoniemi, R. J., Knuutila, J., and Lounasmaa, O. V., Rev. Mod. Physics **65**, 413-497 (1993)
[3] Kraus, Jr., R.H. Flynn, E.R., Overton, W., Espy, M.A., J.S. George, Matlashov, A., Peters, M.A. and Ruminer, P., Recent Advances in Biomagnetism, T. Yoshimoto, et al. Ed., p. 5 (1999); 11th Intl. Conf. Biomagnetism, Sendai, Japan, August 1998.
[4] van Hulsteyn, D.B., Petschek, A.G., Flynn, E. R., and Overton, W.C., Superconducting imaging surface magnetometry, Rev. Sci. Instr. **66**, 3777-3784 (1995)
[5] Meissner, W., Naturwissenschaften, **21**, 787 (1933).
[6] Merr, H., Purcell, A., Stroink, G., "Design of large Helmholtz Coils", Rev. Sci. Instr., **54**, 7 (1983)

Figure Captions—

Fig. 1. Illustration of the FEM mesh used to represent the SIS of our whole-head MEG system. The teal surface shows the distribution of SQUID magnetometers inside the SIS.
Fig. 2. Vector representation of the magnetic field at each SQUID sensor for (2a) a point dipole source located 2m to the right of the SIS helmet, and (2b) a uniform field source outside the SIS.
Fig. 3. Comparison of magnetic field distributions for six representative phantom sources near the apex and edge of the SIS helmet. **1a:** Measured results, and **1b:** FEM model results
Fig. 4. Source localization errors for 25 phantom coils prior to SQUID sensor calibration procedure (see text).
Fig. 5. Source localization error for independent 25 phantom coils after calibrating SQUID sensor positions and sensitivities.

Figure 1:

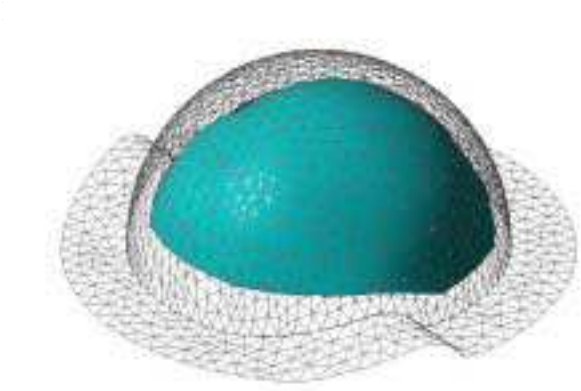

Figure 2a:

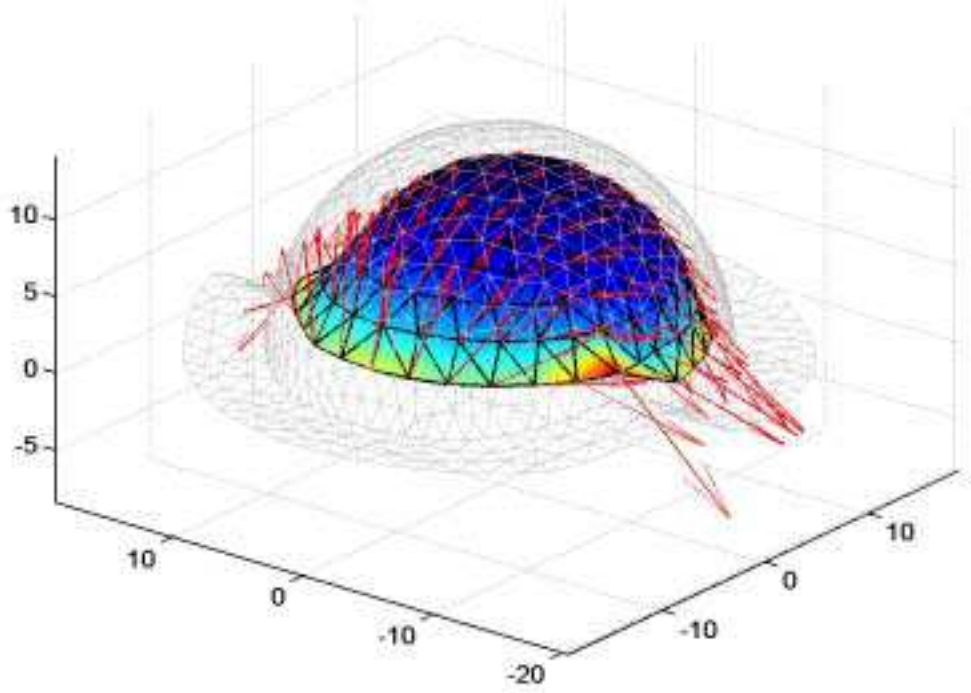

Figure 2b:

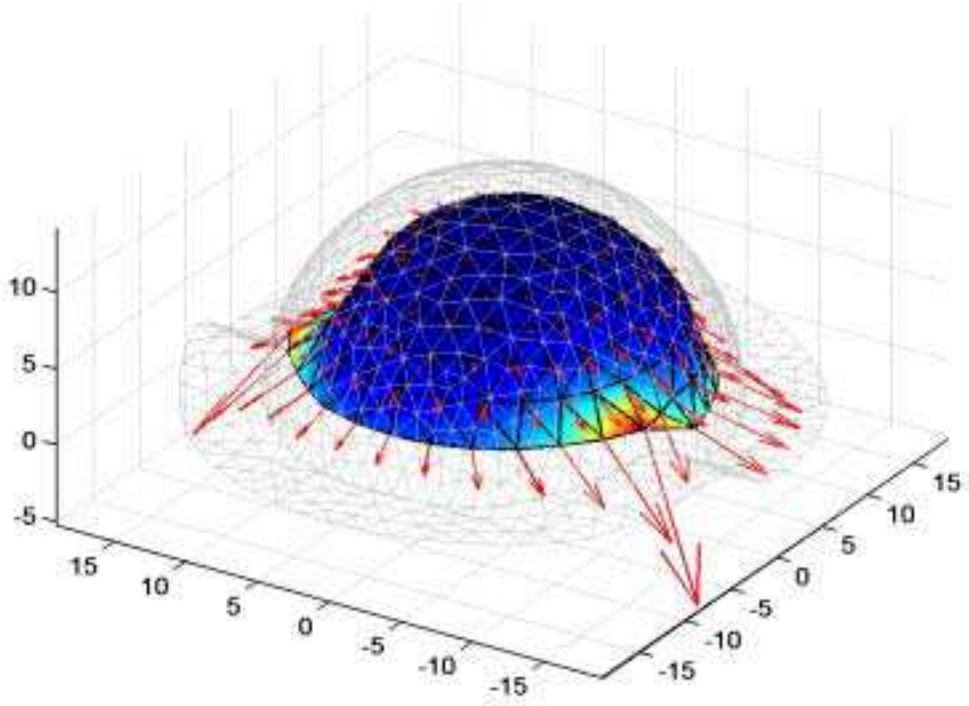

Figure 3a:

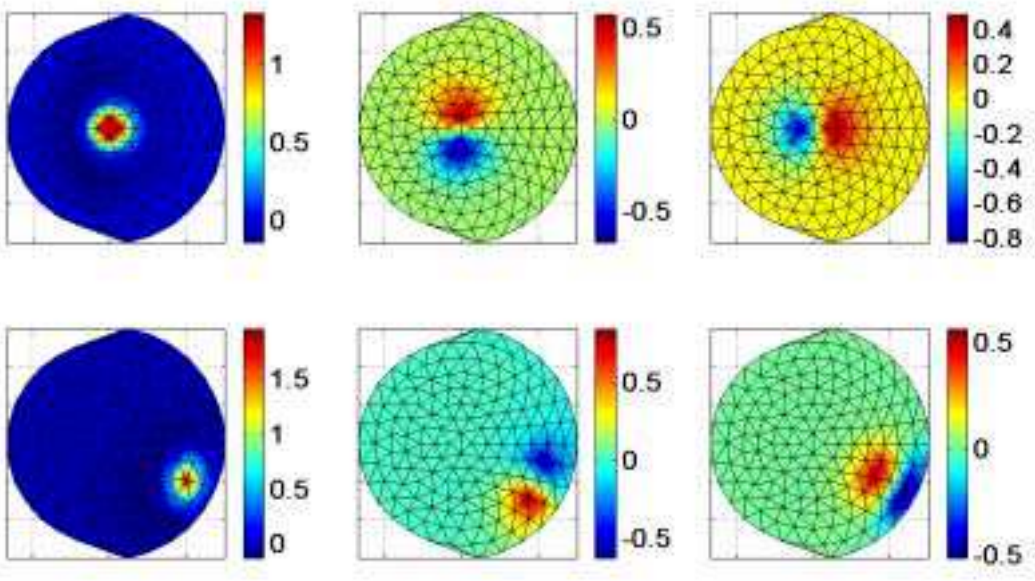

Figure 3b.

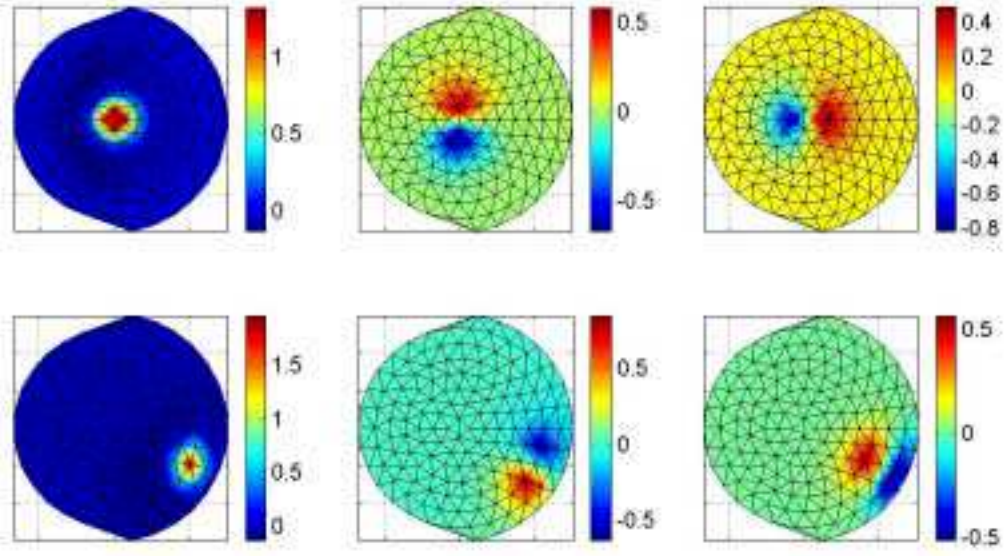

Figure 4

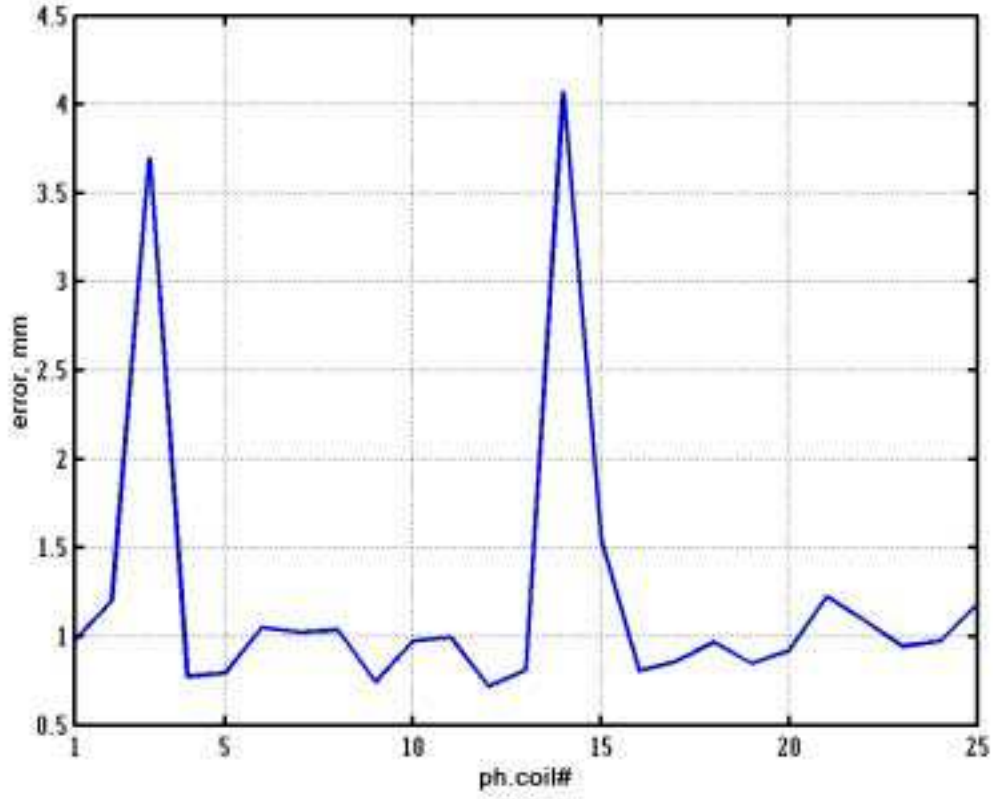

Figure 5